



UNIVERSITY OF LEEDS

This is a repository copy of *Manufacture of poly(methyl methacrylate) microspheres using membrane emulsification*.

White Rose Research Online URL for this paper:
<http://eprints.whiterose.ac.uk/96873/>

Version: Accepted Version

Article:

Bux, J, Manga, MS, Hunter, TN et al. (1 more author) (2016) Manufacture of poly(methyl methacrylate) microspheres using membrane emulsification. *Philosophical Transactions A: Mathematical, Physical and Engineering Sciences*, 374 (2072). 20150134. ISSN 1364-503X

<https://doi.org/10.1098/rsta.2015.0134>

© 2016 The Author(s). Published by The Royal Society. This is an author produced version of a paper published in *Philosophical Transactions A: Mathematical, Physical and Engineering Sciences*. Uploaded in accordance with the publisher's self-archiving policy.

Reuse

Unless indicated otherwise, fulltext items are protected by copyright with all rights reserved. The copyright exception in section 29 of the Copyright, Designs and Patents Act 1988 allows the making of a single copy solely for the purpose of non-commercial research or private study within the limits of fair dealing. The publisher or other rights-holder may allow further reproduction and re-use of this version - refer to the White Rose Research Online record for this item. Where records identify the publisher as the copyright holder, users can verify any specific terms of use on the publisher's website.

Takedown

If you consider content in White Rose Research Online to be in breach of UK law, please notify us by emailing eprints@whiterose.ac.uk including the URL of the record and the reason for the withdrawal request.



eprints@whiterose.ac.uk
<https://eprints.whiterose.ac.uk/>

Manufacture of Poly(methyl methacrylate) Microspheres using Membrane Emulsification

Jaiyana Bux¹, Mohamed S. Manga¹, Timothy N. Hunter¹ and
Simon Biggs^{2*}

1. *Institute of Particle Science and Engineering, School of Chemical and Process Engineering, University of Leeds, Leeds LS2 9JT, UK.*
2. *School of Chemical Engineering, University of Queensland, Brisbane, QLD 4072, Australia.*

Keywords: polymer microspheres, membrane emulsification, suspension polymerisation, poly(methyl methacrylate)

Summary

Accurate control of particle size at relatively narrow polydispersity remains a key challenge in the production of synthetic polymer particles at scale. A cross-flow membrane emulsification [XME] technique was used here in the preparation of poly (methyl methacrylate) [PMMA] microspheres at a 1 – 10 L/h scale, to demonstrate its application for such a manufacturing challenge. XME technology has previously been shown to provide good control over emulsion droplet sizes with careful choice of the operating conditions. We demonstrate here that for an appropriate formulation, equivalent control can be gained for a pre-cursor emulsion in a batch suspension polymerisation process. We report here the influence of key parameters on the emulsification process; we also demonstrate the close correlation in size between the pre-cursor emulsion and the final polymer particles. Two types of polymer particle were produced in this work, a solid microsphere and an oil-filled matrix microcapsule.

Introduction

The range of applications for polymeric microspheres continues to grow across a wide scope of technology areas. In many cases, particles with controlled size characteristics are required. [1] For applications such as particle sizing standards this is self-evident whilst it has long been a requirement for chromatography applications where the particles act as the absorbent stationary phase and variations in surface area effect the retention time in the column.

Over the last few decades, polymer microspheres have found increasing use in biomedical applications. [2] The incorporation of pharmaceutical actives into inert carrier particles is frequently described as a route for novel drug delivery materials; and, the link between drug availability and particle size is now well established, providing further impetus for managing particle sizes accurately. Passage into and through the body is also known to be dependent on particle size, for example inhaler applications have a very tight particle size requirement. [3] Finally, we note that there is an ever-growing interest in microparticles for use in medical imaging applications, where again good size control is a key requirement. [4]

Suspension polymerisation is used industrially for the production of a wide range of important commercial polymers such as polystyrene [PS], poly (methyl methacrylate) [PMMA] and poly (vinyl chloride) [PVA]. It is

*Author for correspondence (simon.biggs@uq.edu.au).

1
2
3
4 also used to produce a range of polymer particles such as ion exchange resins and chromatography beads. For
5 particle synthesis, the size distribution of the final particles is often very similar to that of the original
6 emulsion and so good control over the emulsion may be expected to provide good control over the final
7 particulate product. [5] Industrial production of emulsions is usually achieved using rotor-stator systems,
8 high-pressure homogenisation or ultrasound. In general, these approaches use large quantities of energy and
9 produce emulsions with a wide distribution of sizes. [6] During the emulsification, there will consequently be
10 a large degree of drop break-up and drop coalescence during the process. Where the incorporation of another
11 material into the particles is intended, for example a drug active, this complex process may cause difficulties
12 in ensuring equal dosing in all particles. In a further limitation, these processes typically utilise very high
13 shear conditions that may be detrimental to sensitive active molecules in a pharmaceutical formulation, for
14 example.

15 The production of emulsions using drop-by-drop approaches is of growing interest for a wide range of
16 possible applications as a result of the generally excellent control over droplet size and size distribution
17 available. [2] Examples of such approaches using microfluidic devices as well as controlled pore size
18 membranes have been reported. The advantages of such approaches are many: They are typically low energy;
19 the shear fields are generally weak; exquisite size control is available; almost mono-disperse product can be
20 attained; and, through careful use of multiple systems in sequence, complex droplet-in-droplet architectures
21 can be produced. [6, 7] Despite this, commercial applications based on this technology remain very few: One
22 disadvantage is the generally limited production rates, especially for microfluidic devices. For membrane
23 emulsification systems, as an example, the oil flux for a 0.5 μm Shirasu Porous Glass (SPG) membrane has
24 typical values ranging from 10 – 45 $\text{dm}^3\text{m}^{-2}\text{h}^{-1}$ [8]. Higher fluxes have been reported using ceramic membranes
25 with possibly up to one order of magnitude increase available. Manufacturing approaches that use premix
26 routines and recycling of emulsions can also be used to improve operational efficiency and improve emulsion
27 quality. [9] It is worth noting here that cross-flow membrane [XME] systems of the type used in this work can
28 be easily parallelised to increase production volumes and it is entirely feasible to match the output of an
29 industrial homogeniser with a similar sized unit. [10] Membrane or channel fouling is another potential issue
30 for these drop-by-drop approaches that needs to be carefully managed if they are to be successfully scaled up
31 for manufacturing applications.

32
33 Our work here focuses on the production of PMMA microspheres via a suspension polymerisation process,
34 using a stable pre-prepared emulsion of monomer and initiator dispersed in an aqueous continuous phase.
35 For membrane emulsification, the basic method is very simple in concept; a pressure is applied to one liquid
36 forcing it to permeate through a porous membrane into the continuous phase. A schematic of the process is
37 shown below in Figure 1. As droplets are extruded from the membrane pores, they are detached by a
38 combination of the hydrodynamic forces generated by the cross-flow of the continuous phase, the trans-
39 membrane pressure driving the flux of liquid through the membrane, and the wetting properties of the
40 droplet and continuous phase on the membrane. For membranes with tight pore size distributions it is
41 possible to produce essentially monodisperse emulsions. [6] Empirical relationships between pore size, liquid
42 viscosity, trans-membrane pressure and membrane type allow control over the droplet size. [8] A range of
43 possible materials have been tested for use as membranes, these include glass, ceramics, polycarbonates,
44 micro-laser drilled steel and teflon. [11] The most widely reported system is based on the SPG membranes.
45 These membranes are appealing as the surface wettability can be easily modified and a wide range of pore
46 sizes are available (typically from 0.05 - 30 μm). [12] Regardless of the membrane type it is known that the
47 droplet sizes are usually 2-10x the pore diameter for stable emulsion production. [13]

48
49 Given that it has been previously established that particle sizes from suspension polymerisation closely match
50 those of the initial emulsion droplets, we have elected to explore XME as a route to produce the emulsion.
51 XME utilises a membrane material, in our case a sintered ceramic, with a narrow pore size distribution
52 through which the dispersed phase can be expressed. In principle, a droplet can grow from each of the pores
53 directly into the continuous phase. The stability of a droplet on the membrane is controlled by a balance of the
54 various forces acting on it; and, the detachment point is usually controlled by an imbalance between the
55 Laplace pressure and the shear stress caused by the cross-flowing continuous phase. [11, 14] Earlier work has
56 highlighted the importance of factors such as cross-flow rate, driving pressure, surface tension, and droplet
57
58
59
60

stabilisation by surfactant adsorption during growth and detachment as important for controlling the ultimate droplet size and polydispersity of the end product. [15]

The first demonstrations of membrane emulsification for the production of polymer microspheres were reported by Omi and co-workers in the late 1990s. [12, 16, 17] In this pioneering work, both PS and PMMA microparticles were synthesised from emulsions produced using a porous alumina-silicate glass membrane. Due to difficulties producing a stable MMA emulsion, a more complex 2-stage process with initial emulsification and then subsequent droplet swelling was employed. Despite this, stable dispersions of PMMA particles with diameters ranging from 3 μm to 35 μm were reported with a typical coefficient of variation (CV) at 10%. Later work from the same group describes a single stage process for the emulsification of MMA prior to the subsequent polymerisation reaction although details of what had been modified to achieve this were not provided. [18, 19] We assume here that the wettability of the membrane had been adjusted although this was not explicitly stated. Since these early studies, a number of other reports concerning other polymer materials and/or other polymerisation or particle formation approaches have been published. [2, 9] Despite the breadth of this earlier work, there are only limited studies on the preparation of polymer microspheres and these typically utilise emulsions at relatively low disperse phase volume fractions (5 – 7%), with the polymerisation being undertaken on batch sizes of 300 ml or less. Wolska and Bryjak have reported a process to produce polystyrene microspheres using membrane emulsification where the emulsion was produced at 15% w/w styrene. [20]

In our earlier work, we demonstrated the potential of membrane emulsification for microcapsule manufacture [21]. In the work reported here, we extend this work to produce dispersions of solid poly(methyl methacrylate) particles at a relatively high particle concentration and in considerably larger volumes than has been previously demonstrated in the open literature. Using a sintered ceramic membrane, we aim to develop a simpler formulation and production process that will ultimately facilitate easier scale-up to industrial levels. Two types of particle were examined in this work: A solid polymer microsphere and an oil-filled matrix microcapsule type of particle.

Materials and Methods

Chemicals

Methyl methacrylate monomer (Sigma Aldrich, 30 ppm) was passed through an alumina column to remove inhibitors and then stored in a refrigerator prior to use. Benzoyl peroxide [BPO] (Alfa Aesar, 25% moisture content), an oil soluble initiator; lauryl alcohol [LA] (Sigma Aldrich, 98%); sodium dodecyl sulphate [SDS] (Sigma Aldrich, 98%); and, Mowiol (polyvinyl alcohol 8-88) [PVA] (Sigma Aldrich, degree of polymerisation ~1,400, 86.7 – 87.7 mol% hydrolysis, molecular weight ~67,000) were all used as supplied. Hydroquinone (Alfa Aesar, 99%) was used as an inhibitor to control secondary nucleation and was also used as supplied. Castor oil (Fluka, 100%) was used as received. All water used here was of Millipore Milli-Q grade.

Cross-flow membrane emulsification

Emulsions were prepared using a cross-flow membrane (XME) method. The membranes used in the work reported here were multi-channel ceramic tubes, as shown in Figure 1. These alumina-coated membranes were specially commissioned (Fairey Industrial Ceramics Ltd., UK) and had average pore sizes of 0.2, 3 and 10 μm , respectively, on the detachment surfaces. The tubular membranes have a 600 mm length and an external diameter of 20 mm, in each case they have 7 star-shaped channels into which the disperse phase is expressed. Surface porosity has previously been reported as 10% [22] with a pore size span of 0.3 – 0.8 (see below).

The ceramic membrane of choice is housed in a stainless steel module that allows the continuous phase to be pumped along the inner surfaces of the membrane creating a shear field on those surfaces. The disperse phase is then pushed under pressure through the membrane from the external surface into the inner channels where oil droplets form at the membrane pores. The droplets will then grow and eventually detach under the action

of the shear force caused by the cross-flowing continuous phase. The emulsion is usually re-circulated through the system using a pump until the desired emulsion concentration is achieved. The conditions used in the XME during production, such as the cross-flow rate and the pressure used to force the disperse phase through the membrane, can be tightly controlled.

All emulsions were produced at room temperature (20 ± 1 °C) and, in each experimental sample, the continuous phase was re-circulated through the system whilst the disperse phase was expressed resulting in a final emulsion with a droplet concentration of ~ 30% w/w. Emulsions samples were analysed using laser light scattering for droplet size and size distribution.

Suspension Polymerisation

Suspension polymerisation protocols were initially based on those of Omi et al [16, 17]. Prior to running a large-scale batch polymerisation capable of accepting the full volume produced by the XME system, a series of small batch polymerisations were performed in a Carousel-6 reactor with a Tornado overhead stirrer (Radleys Ltd., UK) to optimise the formulation for use here. The formulation recipes tested are given in Table 1. For each formulation, a batch of emulsion was pre-prepared using the XME system, with a 3 µm pore size membrane. After loading small batches (200 g) into the reactor, all samples were purged with Nitrogen and the temperature was raised to 65°C, which is sufficient to cause the breakdown of BPO and the formation of free radicals to initiate the polymerisation. For scale up of the suspension polymerisation, an approximately 2.4 Kg batch of the preferred emulsion formulation was prepared using XME at 30% w/w MMA. Details of the Formulation recipe are given in Table 2. A 900 g sample batch of this emulsion was transferred to a jacketed reactor vessel equipped with an overhead stirrer and a condenser. Prior to initiation of the polymerisation reaction, the emulsion was diluted with water (1823 g) and PVA (12.2 g) to give a final emulsion weight of 1.8 Kg (i.e. ~ 16% w/w MMA). This was done primarily to manage the viscosity in the reactor and to prevent the formation of excess coagulum around the stirrer. Once again, the emulsion was purged with nitrogen and then heated to 65°C to initiate the reaction.

In an alternative formulation, the MMA was partially replaced with Castor oil to explore the potential of this approach for producing oil-filled microcapsules. Samples ranging from 6 wt% to 24 wt% castor oil, within the oil phase were prepared.

For all polymerisation reactions, final conversions were determined gravimetrically. The sample weight was recorded for the wet suspension. Subsequently it was dried in an oven at 70 °C for 8 hours and reweighed.

Emulsion and Particle Characterisation

A Malvern Mastersizer 2000 (Malvern Instruments Ltd., UK) equipped with a Hydro S dispersion cell was used here for size analysis of particle and emulsion samples. Typically, a small sample was dispersed into a bath of water within the dispersion cell and then circulated through the measurement cell. Sample concentration was adjusted until an appropriate obscuration was achieved. The Mastersizer produces a particle size distribution from the low angle scattering pattern using a conversion algorithm based on Mie theory. Each sample run consists of 10 measurements and the reported size and size distribution data are an average of these multiple measurements.

Data are reported from the equipment as the D10, D50 and D90 which correspond to the droplet diameters at 10%, 50% and 90% of the total volume, respectively. Size distribution is reported as the span where:

$$span = \frac{D_{90} - D_{10}}{D_{50}}$$

Zeta potential data as a function of pH, for the PMMA latex particles, were analysed using a Malvern ZetaSizer nano instrument.

Polymer particles were observed with a Carl Zeiss EVO MA15 scanning electron microscope (Carl Zeiss Ltd, UK). Care was taken to ensure that the beam intensity did not lead to particle melting.

Results and Discussion

Formulation Optimisation

In earlier work [17], hydroquinone was added to the aqueous phase to prevent the formation of particles from soluble monomer in the continuous phase. Other salts, such as sodium sulphate tested here, were also used to control the pH. In the formulation tests conducted here, the small batch polymerisations were always unsuccessful in the presence of hydroquinone. Interestingly, the simplest formulations tested (Table 1: #1 and #2) gave the most reliable polymerisation results and were therefore chosen as the base for further investigation with membrane emulsification. During the scale-up, it was decided to increase the SDS concentration (Table 2) to ensure that the formulation was well above the critical micelle concentration. We also added PVA to enhance the stability of the final particle sample.

Emulsion formation

Table 3 summarises the experimental conditions and the associated size information for the emulsions produced here by membrane emulsification (ME).

Looking first at the emulsions produced with the smallest pore size membrane (0.2 μm), we can examine the effects of various operational parameters. (X)ME is known to be sensitive to the interplay between a wide range of operational and materials parameters, including: The cross-flow shear field; the cross-membrane pressure; the wettability (of both phases) on the membrane; the viscosity of both phases; densities; and, the interfacial tension. [11, 23] Furthermore, the shape, spatial location, and spacing of the pores can also have a significant influence. [22] Despite many empirical studies using a wide variety of each of these parameters, and various computational investigations [24, 25], no fully predictive rules for this process are available. It is pertinent then to optimise the process using the preferred formulation for the polymerisation reactions.

In a drop-by-drop emulsification process, the growth and detachment of a droplet from the mouth of a pore is controlled (primarily) by the balance between the interfacial tension force (resistance) and the drag force from the cross-flowing continuous phase (detachment). Any buoyancy forces are deemed to be negligible. [25] Should the inertial force due to the disperse phase emerging from the pore become larger than the interfacial tension force then we would transition from 'dripping' to 'jetting' behaviour. [27] In practice, for most ME equipment, this transition point is never reached and 'dripping' behaviour is dominant. A simple force balance model can be used to show that [28]:

$$R_d/R_p \propto (Ca)^{-1/2}$$

Where R_d and R_p are the droplet and pore radii, respectively, and Ca is the capillary number which defines the ratio between the interfacial tension and drag forces, where;

$$Ca = \frac{\eta \cdot v_c}{\gamma}$$

and, γ is the interfacial tension, η is the viscosity and v_c is the *continuous* phase velocity (taken as the average cross-flow velocity). The transition from dripping to jetting is frequently described through a regime map that plots the continuous phase Capillary number against a disperse phase Weber number [27], where;

$$We = \frac{d \cdot r \cdot v_d}{\gamma}$$

v_d is the *disperse* phase injection velocity and d is the fluid density whilst r is the pore radius. The injection velocity was calculated from the measured disperse phase flux, where it was estimated that 5% of the total pore surface area was accessible. Given the relatively low pressures and small pore sizes, this active area was an average value from previous literature [29], although it was not measured directly and may not be constant across the different pore sizes used.

In Figure 2, data for the droplet size distributions as a function of the cross-membrane pressure are given for the 0.2 μm pore membrane. A cross-flow velocity in the continuous phase of 2 m/s is used in each case. We see here a general shift to a larger mean size as the membrane pressure is increased, consistent with previous investigations. This increase in size with an increase in membrane pressure has previously been rationalised on the basis of dynamic interfacial tensions. It is postulated that, at the higher pressures, the rapidly expanding interface of a growing drop is insufficiently coated with surfactant and so the dynamic surface tension is higher. [30] This leads to increased stability of the droplet at the membrane surface and a corresponding increased growth prior to detachment. The measured span values at 0.3 and 0.1 MPa are 1.4 and 1.2, respectively. This small increase in the span at higher pressure may be due to the increased number of active pores at the higher pressure: At higher cross-membrane pressures more smaller pores will be active as their capillary pressures are exceeded. [29]

Interestingly, at the lowest membrane pressure tested here, 0.05 MPa, we see a bimodal distribution in the size data. This is consistent with the formation of satellite droplets during droplet detachment from the membrane and suggests a more complex process than is often described for the droplet formation/detachment. [30] Various computational fluid dynamics (CFD) and Lattice Boltzmann (LB) simulations have shown how droplets growing at a membrane pore become distorted in the direction of the cross-flow. [28, 32] In this case, the slower growth of the interface should result in a lower dynamic interfacial tension with an associated smaller mean drop size, as is seen. However, the reduced interfacial tension will also allow a greater distortion of the growing drop within the cross-flow shear field. This distortion may lead to an elongation of the droplet and, under certain conditions, the formation of a capillary neck that eventually breaks releasing the main drop. The breaking of the neck and the associated snap back to the pore may also give rise to a satellite drop, a well understood hydrodynamic phenomenon. The relatively narrow distribution of drop and satellite sizes suggest that, in this case, the formation process is still highly reproducible.

In Figure 3, data for the droplet size distributions as a function of the continuous phase cross-flow rate are given, with all other operational parameters being held constant and a membrane pressure of 0.3 MPa being used. We see here a reduction in the mean size as a function of increased cross-flow rate that is consistent with many earlier studies. Again, from a simple force balance model we may expect that as the drag force increases the droplets will detach sooner and at a smaller mean size, as is seen. At the lower cross-flow rates tested here, we also see essentially bimodal size distributions. Once again, the possibility for the formation of satellite drops being produced during detachment needs to be considered. Here, the droplets are expected to grow to a larger mean size in the lower shear field; these larger droplets will be more deformable as a result of a lower Laplace pressure and may elongate more in the direction of the cross-flow. It is also noteworthy that the mean drop sizes (largest peak) at these low cross-flow rates are 20 – 30 \times the pore size, consistent with considerable distortion of the droplet. [28] Previous modelling has shown that the drag force is reduced as the droplet deforms, allowing for further growth of the droplet prior to detachment.

The effects of increasing the viscosity of the disperse phase on the droplet size distributions are shown in Figure 4. In this example, increased percentages of castor oil are added to the MMA in the disperse phase. The viscosities of the MMA and castor oil are 0.6 and 650 mPa.s, respectively, at 20°C. Clearly, the addition of the castor oil will significantly increase the viscosity of the oil phase. In the data shown in Figure 4 we see that an increase in the castor oil content leads to an increase in the droplet mean size; in all cases, the size distribution is monomodal with a relatively narrow CV. This increase in the mean size correlates with an increased stiffness of the droplets at the membrane surface. It has previously been shown that changing the ratio of disperse phase to continuous phase viscosities leads in some cases to an increase in droplet size, as seen here,

whilst in other examples the opposite effect occurs. [33] An increase in drop stiffness might be expected to lead to a higher drag force and a resultant decrease in size; clearly a complicating effect must be prevalent here although it is not clear what that might be. We note that the interfacial tension of MMA-water and castor oil-water are both around 15 mN/m and so we do not expect a large change in interfacial tension with changing oil composition.

Oil flux is obviously important for determination of the overall emulsion production rate, which is important for longer-term interest in this technology as a manufacturing route for large volumes of emulsions or particulates. Simple calculations suggest that for oil flux rates of up to 50 L /m².h used here with a 0.2 µm membrane, we can expect to produce around 7.5L of emulsion per hour. This should be compared with an industrial homogeniser which can produce around 1 m³ h⁻¹. It has previously been postulated that this production challenge could be solved by the design of an emulsifier with an array of ceramic tubes in parallel. [33] We note here that such a design has yet to be demonstrated.

Another route to increase the oil flux and improve the production rate is to use a membrane with a larger pore size. Data for the size distribution as a function of the cross-membrane pressure are shown in Figure 5 for a membrane with a 3 µm pore size. In this case, low oil flux leads to an emulsion with a very polydisperse droplet size. An essentially monomodal distribution with a low span is seen at a membrane pressure of 0.23 MPa. Interestingly, the median size for this sample is D50 = 2.0 µm, which is less than, but close to, the mean pore size. In contrast with the data for the small pore membrane (above), the broadening of the size distribution for this membrane is towards larger droplets as the pressure is decreased. The most plausible explanation for this would seem to be as a result of coalescence between droplets from neighbouring pores on the membrane.

As the pore size is increased, the cross-membrane pressure needed to activate a given pore is reduced and so we may expect more pores to be active at all times. Previous research has suggested that < 10% of pores are active at any time for the 0.2 µm membranes used here. [29] However, for the 3 µm pore size membranes, at a similar cross-membrane pressure and for a similar formulation, we can expect that a larger fraction of the pores are active. Obviously, if more pores are active then the mean distance between two growing drops on the membrane surface at any given time will be reduced and the possibility of neighbouring drops interacting will be increased. Also, as the pore size increases then the expected drop size will also increase and larger drops have a lower Laplace pressure and are more deformable. We can expect considerable deformation in the direction of the cross-flowing continuous phase with the associated reduction in drag force leading to larger drop sizes, as discussed above. In addition, larger drops, with the associated deformation, may facilitate coalescence between neighbouring drops. All of this is consistent with the polydisperse droplet size distributions recorded for the lower pressures in this case.

These arguments do not, however, explain the relatively small droplet size and monomodal size distribution seen for the highest cross-membrane pressure tested here. When the number of active pores is very high but where coalescence is somehow prevented, possibly by surfactant adsorption, an additional detachment mechanism has been suggested by Holdich and co-workers. [34] This so-called 'push-off force' relies on the deformation of growing drops at adjacent pores. This deformed ellipsoidal shape increases the free energy of the droplet; detachment leads to the drops reverting to a spherical shape and a reduction in the free energy. The steric hindrance of neighbouring drops also prevents deformation in the direction of flow further reducing the growth of the droplets. The addition of a push-off force when added to the drag force from the cross-flow results in the detachment of droplets from the membrane surface at smaller than predicted sizes. Whilst we hypothesise that this effect may be occurring here, it is worth noting that previous reports of this effect have been with straight-through drilled steel membranes where the pore activity is typically very high and can approach 100%. It has been suggested that this effect would be much less likely on a glass or ceramic membrane where pore activity is usually lower. [35]

Another possible explanation is that we are operating in a jetting regime rather than the classical dripping one more common with these systems. It has been shown previously that controlled jetting can give rise to droplets with narrow polydispersity in size. [36] Furthermore, these droplets typically have a mean size that is smaller than the pore dimensions. Previously, it has been claimed that an oil flux of > 100 L/m².h through *Phil. Trans. R. Soc. A.*

these ceramic membranes leads to unstable conditions and a possible loss of control in the droplet polydispersity. [6] Looking at the disperse phase flux values used here (Table 3), we see that for the 3 μm membrane example we are either close to, or significantly exceed this value. Interestingly, under the conditions where we significantly exceed this flux value we see the highest quality of droplet formation, i.e. lowest polydispersity: A similar outcome, at equivalent flux rates, was previously reported by Yuan et al when using the same experimental set-up as we employed here. [21] The conditions for a transition from dripping to jetting behaviour have previously been defined in terms of dimensionless hydrodynamic numbers; specifically, the Weber number for the disperse phase and the capillary number for the continuous phase. [25, 27, 35] Looking at these predictions, Meyer and Crocker [27] suggest that for $\text{Ca} > 10^2$ we can enter a jetting regime even for $\text{We} < 10^2$ (and a clear jetting regime for We above this value). Comparing our conditions to these dimensionless numbers for the experiments run here (Table 3), we see that all data for the 0.2 μm pore membrane are within the dripping regime whereas the data for the 3 μm pore membrane are close to or beyond the boundary with the jetting regime. It seems entirely feasible here that we are operating under conditions where jetting is dominant and where most of the pores are active. In the case of jetting, droplets will form downstream of the pore through Rayleigh instabilities within the jet that cause its break-up. This results in very rapid emulsification but, importantly, whilst still retaining reasonable control over the droplet properties. Further work is required to better understand these observations from our work. Data for a 10 μm pore membrane are also given in Table 3 for a single emulsification run. Here, we expect to be very strongly within a jetting regime. The size distribution data (not shown here) is again monomodal with a relatively narrow distribution; in this case, however, the median drop size is approximately one third of the pore dimension. It is interesting that we retain a relatively good control on the emulsion properties even under these conditions.

Looking at the oil flux data for the 3 μm membrane, we can calculate an emulsion production rate in excess of 3500 $\text{L}/\text{m}^2\cdot\text{h}$ or around 500 L/h on a single membrane channel. This compares much more favourably with the output of a homogeniser than the examples for the 0.2 μm membrane above. As noted before, a set of membranes in parallel could, in principle increase the production rate very simply. [21] Obviously, issues associated with consistent pressures across all the membranes and equalised cross-flow conditions would need careful design. To date, very little work on this up scaling has been done and it would seem timely that more attention is now given to this subject although this is beyond the scope of our current work.

Particle Synthesis

Size distribution data for particle samples and relevant pre-cursor emulsions prepared with both the 0.2 and 3 μm membranes are given in Figures 6 and 7, respectively. It is clear that the particle size distribution matches closely the pre-cursor oil monomer droplet characteristics in both cases. This is consistent with a number of earlier studies concerning the use of membrane emulsification technologies for the preparation of precursor droplets in a suspension polymerisation process. [16 - 20] The absence of agglomeration between droplets/particles during the polymerisation process suggests that the added PVA is effective as a steric stabiliser. This control is very promising for the future and suggests that we can gain good control over the eventual particle sizes through control of the emulsion production. Interestingly, there does appear to be a small shoulder in the particle size distribution that is not seen in the emulsion pre-cursor. It is not clear, at this time, what may have lead to the appearance of this smaller size fraction.

For both the solid polymer particles and the microcapsules, the conversion of monomer to polymer was calculated to be $> 85\%$ w/w. SEM images of the solid polymer microspheres are given in Figure 8. It is evident from these images that the surface of the microspheres for both the solid particles and the oil-filled capsules is essentially smooth. Interestingly, we see no evidence for the formation of small particulates in the continuous phase as a result of secondary nucleation reactions despite the removal of the hydroquinone from our formulation: In the earlier work of Omi and co-workers [16, 17] small particles from such a secondary nucleation process were seen from SEM images to decorate the larger particles. Although not shown here, TEM analyses of the microcapsule samples confirmed the inclusion of the oil within the particles in a matrix type structure.

Zeta potential data (Figure 9) for the solid PMMA particles provides additional information about their surface properties. As expected the particles are highly negatively charged and stable, primarily through the adsorption of the SDS, with the magnitude only reducing at very low pH near the isoelectric point. With the addition of increasing concentrations of salt, the zeta-potential of the particles is increasingly reduced at each pH, destabilising the dispersion almost completely at 10^{-2} M (as the particle charge is almost completely suppressed here). Whilst we expect some steric stabilisation from the adsorption of the PVA, destabilisation at the higher salt concentration suggests that this is inefficient.

Conclusions

We have successfully demonstrated a two-stage approach for the manufacture of polymer microspheres with good control over the mean particle size and the associated size distribution. A thermally initiated suspension polymerisation reaction followed the formation of a precursor emulsion of monomer (and oil-soluble initiator) in water produced using membrane emulsification. A close correlation between the precursor emulsion droplets and resultant particle size distributions was found suggesting that this approach could be used to gain very fine size control over polymer microsphere manufacturing. An analysis of the emulsification process highlighted how the complex interplay between materials and membrane properties as well as processing conditions must be understood on a system-by-system basis. It is also apparent from this work that much more still needs to be done to fully understand droplet formation and detachment mechanisms from ceramic membranes of the type used in this work.

Additional Information

Funding Statement.

Jaiyana Bux is primarily funded by an Engineering Physical Sciences Research Council (EPSRC)-Nuclear Decommissioning Authority Industrial CASE award managed by the National Nuclear Laboratory.

Timothy Hunter, Mohamed Manga and Simon Biggs were supported by The University of Leeds.

Data Accessibility

Supporting data for this article can be located at <http://espace.library.uq.edu.au/view/UQ:376045>

Competing Interests

We have no competing interests.

Authors' Contributions

Jaiyana Bux is a PhD student and was primarily responsible for the collection of all data reported here and its initial analysis as well as aspects of the experimental design. She also contributed by reading the manuscript and suggesting revisions during its preparation as well as giving final approval.

Mohamed Manga contributed to the experimental design as well as data analysis. He also contributed by reading the manuscript and suggesting revisions during its preparation as well as giving final approval.

Timothy Hunter contributed to the analysis and interpretation of the data along with critical revisions to the draft manuscript. He also gave approval to the final version of the paper.

Simon Biggs is group leader for the research and was a leading contributor to the conceptual design of the experimental program. He was also the primary author of the article responsible for various drafts and final approval.

1
2
3
4
5
6
7
8
9
10
11
12
13
14
15
16
17
18
19
20
21
22
23
24
25
26
27
28
29
30
31
32
33
34
35
36
37
38
39
40
41
42
43
44
45
46
47
48
49
50
51
52
53
54
55
56
57
58
59
60

For Review Only

References

1. Wang, W., Zhang, M-J. & Chu, L-Y. 2014. Functional Polymeric Microparticles Engineered from Controllable Microfluidic Emulsions. *Acc. Chem. Res.* **47**, 373-384. (doi 10.1021/ar4001263)
2. De La Vega, J. C., Elischer, P. Schneider, T. & Häfeli, U. O. 2013. Uniform polymer microspheres: monodispersity criteria, methods of formation and applications. *Nanomedicine* **8**, 265-285. (doi 10.2217/NNM.12.210)
3. Yang, M. Y., Chan, J. G. Y. & Chan, H-K. 2014. Pulmonary drug delivery by powder aerosols. *J. Control. Release* **193**, 228-240. (doi 10.1016/j.jconrel.2014.04.055)
4. Fröhlich, E. 2012 The role of surface charge in cellular uptake and cytotoxicity of medical nanoparticles. *Int. J. Nanomedicine* **7**, 5577-5591. (doi 10.2147/IJN.S36111)
5. Brooks, B.W. 2010 Suspension Polymerization Processes. *Chem. Eng. Technol.* **33**, 1737-1744. (doi 10.1002/ceat.201000210)
6. Vladisavljevic, G. T. & Williams, R. A. 2005. Recent developments in manufacturing emulsions and particulate products using membranes. *Adv. Coll. Inter. Sci.* **113**, 1-20. (doi 10.1016/j.cis.2004.10.002)
7. Zhang, M-J., Wang, W., Yang, X-L., Ma, B., Liu, Y-M., Xie, R., Ju, X-J., Liu, Z. & Chu, L-Y. 2015. Uniform microparticles with controllable highly interconnected hierarchical porous structure. *ACS Appl. Mater. Interfaces* **7**, 13758-13767. (doi 10.1021/acsami.5b01031)
8. Charcosset, C., Limayem, I. & Fessi, H. 2004. The membrane emulsification process – a review. *J. Chem. Tech. Biotech.* **79**, 209-218. (doi 10.1002/jctb.969)
9. Piacentini, E., Drioli, E. & Giorno, L. 2014. Membrane emulsification technology: Twenty-five years of inventions and research through patent survey. *J. Membr. Sci.* **468**, 410-422. (doi 10.1016/j.memsci.2014.05.0519)
11. Hancocks, R.D., Spyropoulos, F. & Norton, I.T. 2013. Comparisons between membranes for use in cross flow membrane emulsification. *J. Food Eng.* **116**, 382-389. (doi 10.1016/j.jfoodeng.2012.11.032)
12. Ma, G. 2002. Control of Polymer particle size using porous glass membrane emulsification. *China Particuology.* **1**, 105-113.
13. Omi, S. 1996. Preparation of monodisperse microspheres using the Shirasu porous glass emulsification technique. *Coll. Surf. A.* **109**, 97-107. (doi 10.1016/0927-7757(95)03477-3)
14. Williams, R.A., Peng, S.J., Wheeler, D.A., Morley, N.C., Taylor, D., Whalley, M. & Houldsworth, D.W. 1998. Controlled production of emulsions using a crossflow membrane part II: Industrial scale manufacture. *Chem. Eng. Res. Des.* **76**, 902-910. (doi 10.1205/026387698525702)
15. Charcosset, C. 2012. Membranes for the preparation of emulsions and particles. In *Membrane Processes in Biotechnology and Pharmaceuticals*, Chapter 6, pp.213-251. Elsevier. (doi 10.1016/B978-0-444-56334-7.00006-X)
16. Omi, S., Katami, K., Yamamoto, A. & Iso, M. 1994. Synthesis of polymeric microspheres employing SPG emulsification technique. *J. Appl. Polym. Sci.* **51**, 1-11. (doi 10.1002/app.1994.070510101)
17. Omi, S., Katami, K., Taguchi, T., Kaneko, K. & Iso, M. 1995. Synthesis of uniform PMMA microspheres employing modified SPG emulsification technique. *J. Appl. Polym. Sci.* **57**, 1013-1024. (doi 10.1002/app.1995.070570814)
18. Nuisin, R., Omi, S. & Kiatkamjornwong, S. 2003. Synthesis and property behavior of dioctyl phthalate plasticized styrene-acrylate particles by Shirasu porous glass emulsification and subsequent suspension copolymerization. *J. Appl. Polym. Sci.* **90**, 3037-3050. (doi 10.1002/app.13032)
19. Nuisin, R., Omi, S. & Kiatkamjornwong, S. 2006. The effects of acrylate monomers and polystyrene addition on the morphology of DOP-plasticized styrene-acrylate polymer particles prepared by SPG emulsification and suspension polymerization. *J. Appl. Polym. Sci.* **99**, 1195-1206. (doi 10.1002/app.22595)
20. Wolska, J. & Bryjak, M. 2009. Preparation of poly(styrene-co-divinylbenzene) microspheres by membrane emulsification. *Desalination.* **241**, 331-336. (doi 10.1016/j.desal.2008.01.070)
21. Yuan, Q.C., Hou, R.Z., Aryanti, N., Williams, R.A., Biggs, S., Lawson, S., Silgram, H., Sarkar, M. & Birch, R. 2008. Manufacture of controlled emulsions and particulates using membrane emulsification. *Desalination.* **224**, 215-220. (doi 10.1016/j.desal.2007.02.095)
22. Yuan, Q., Aryanti, N., Gutiérrez, G. & Williams, R.A. 2009. Enhancing the throughput of membrane emulsification techniques to manufacture functional particles. *Ind. Eng. Chem. Res.* **48**, 8872-8880. (doi 10.1021/ie80112a011)
23. Candéa, T., Monteiro, F.S., Tonon, R.V. & Cabral, L.M.C. 2015. Effect of process variables on the production of flaxseed oil emulsions by cross-flow membrane emulsification. *Food Eng. Rev.* **7**, 258-264.

(doi 10.1007/s12393-014-9085-8)

24. Abrahamse, A.J., van der Padt, A., Boom, R.M. & de Heij, W.B.C. 2001. Process fundamentals of membrane emulsification: Simulation with CFD. *AIChE J.* **47**, 1285-1291. (doi)
25. Pathak, M. 2011. Numerical simulation of membrane emulsification: Effect of flow properties in the transition from dripping to jetting. *J. Membr. Sci.* **382**, 166-176. (doi 10.1016/j.memsci.2011.08.005)
26. Peng, S.J. & Williams, R.A. 1998. Controlled production of emulsions using a crossflow membrane part I: Droplet formation from a single pore. *Chem. Eng. Res. Des.* **76**, 894-901. (doi 10.1205/026387698525694)
27. Meyer, R.F. & Crocker, J.C. 2009. Universal dripping and jetting in a transverse shear flow. *Phys. Rev. Lett.* **102**, 194501. (doi 10.1103/PhysRevLett.102.194501)
28. Boom, R.M. 2007. Emulsions: Principles and Preparation. In *Food Materials Science: Principles and Practice* (eds. Aguilera, J.M. & Lillford, P.J.), Chapter 15. Springer.
29. Lepercq-Bost, E., Giorgi, M-L., Isambert, A. & Arnaud, C. 2008. Use of the capillary number for the prediction of droplet size in membrane emulsification. *J. Membr. Sci.* **314**, 76-89. (doi 10.1016/j.memsci.2008.01.023)
30. Schröder, V., Behrend, O. & Schubert, H. 1998. Effect of dynamic interfacial tension on the emulsification process using microporous ceramic membranes. *J. Coll. Inter. Sci.* **202**, 334-340. (doi 10.1006/jcis.1998.5429)
31. Kosvintsev, S.R., Gasparini, G. & Holdich, R.G. 2008. Membrane emulsification: Droplet size and uniformity in the absence of surface shear. *J. Membr. Sci.* **313**, 182-189. (doi 10.1016/j.memsci.2008.01.009)
32. Pathak, M. 2012. Numerical simulation of droplet dynamics in membrane emulsification systems. In *Numerical Simulation – From Theory to Industry* (Ed. Andriychuk, M.), Chapter 19, pp. 415-438. Intech Open.
33. Feigl K., Tanner, F.X., Holzapfel, S. & Windhab, E.J. 2014. Effect of flow type, channel height, and viscosity and drop production from micro-pores. *Chem. Eng. Sci.* **116**, 372-382. (doi 10.1016/j.ces.2014.05.015)
34. Holdich, R. G., Dragosavac, M. M., Vladislavljevic, G. T. & Kosvintsev, S. R. 2010. Membrane emulsification with oscillating and stationary membranes. *Ind. Eng. Chem. Res.*, **49**, 3810–3817. (doi 10.1021/ie900531n)
35. Spyropoulos, F., Lloyd, D.M., Hancocks, R.D. & Pawlik, A.K. 2013. Advances in membrane emulsification. Part B: Recent developments in modeling and scale-up approaches. *J. Sci. Food Agric.* **94**, 628-638. (doi 10.1002/jsfa.6643)
36. Böhmer, M.R., Schroeders, R., Steenbakkers, J.A.M., de Winter, S.H.P.M., Duineveld, P.A., Lub, J., Nijssen, W.P.M., Pikkemaat, J.A. & Stapert, H.R. 2006. Preparation of monodisperse polymer particles and capsules by ink-jet printing. *Coll. Surf. A.* **289**, 96-104. (doi 10.1016/j.colsurfa.2006.04.011)

Figure & Table Captions

Figure 1. Images of a typical ceramic membrane used here showing the star-shaped 7 internal channels through which the continuous phase flows.

Figure 2. Droplet size distribution data for three emulsion samples (Table 3: A, B & C) produced using a 0.2 μm pore membrane with a fixed velocity for the cross-flowing continuous phase of 2 m/s, and at different cross-membrane pressures, as shown.

Figure 3. Droplet size distribution data for four emulsion samples (Table 3: C, D, E & F) produced using a 0.2 μm pore membrane with a fixed cross-membrane pressure of 0.3 MPa, and at four cross-flow velocities for the continuous phase, as shown.

Figure 4. Droplet size distribution data for four emulsion samples (Table 3: G, H, I & J) with differing ratios of MMA to castor oil (as shown) produced at fixed cross-membrane pressure and continuous phase cross-flow conditions.

Figure 5. Droplet size distribution data for three emulsion samples (Table 3: K, L & M) produced using a 3 μm pore membrane with a fixed velocity for the cross-flowing continuous phase of 2 m/s, and at different cross-membrane pressures, as shown.

Figure 6. Size distribution data for PMMA/CO microcapsule particle samples and relevant pre-cursor emulsions produced using a 0.2 μm pore membrane (Table 3: I & J).

Figure 7. Size distribution data for a solid PMMA particle sample and the corresponding pre-cursor emulsion produced using a 3 μm pore membrane (Table 3: M).

Figure 8. SEM micrographs of: (a) PMMA/CO microcapsule sample at 12% w/w CO; and, (b) a solid PMMA particle sample.

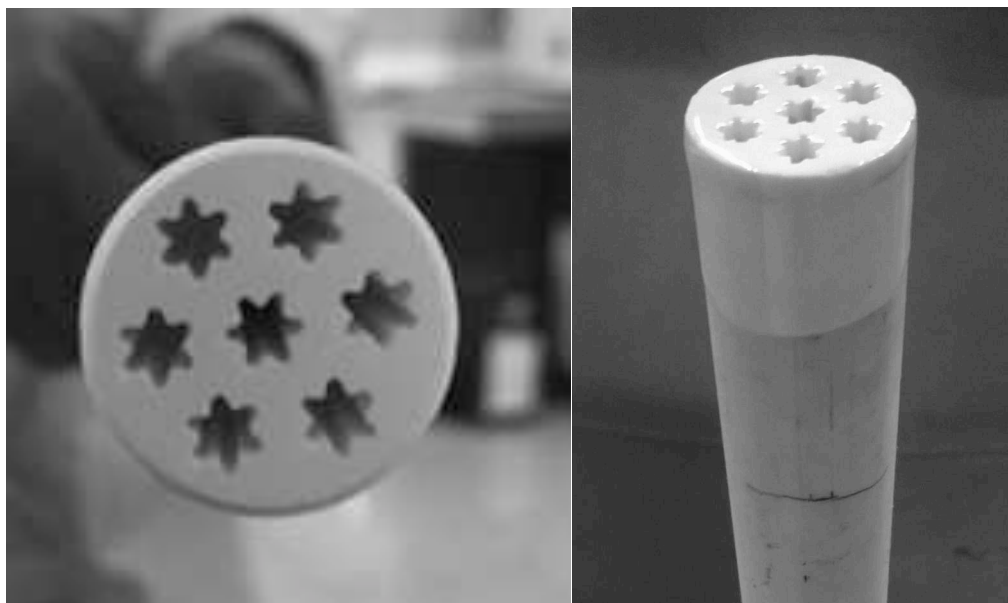
Figure 9. Zeta potential as a function of pH for the solid PMMA particle sample at three different background salt concentrations as marked on the figure.

Table 1. Formulation details for the different small batch suspension polymerisations undertaken in this work.

Table 2. Base polymerisation formulation used in large scale tests.

Table 3. Details of the experimental test conditions and resultant emulsion droplet properties for the cross-flow emulsification tests.

Figure 1:



Review Only

1
2
3
4
5
6
7
8
9
10
11
12
13
14
15
16
17
18
19
20
21
22
23
24
25
26
27
28
29
30
31
32
33
34
35
36
37
38
39
40
41
42
43
44
45
46
47
48
49
50
51
52
53
54
55
56
57
58
59
60

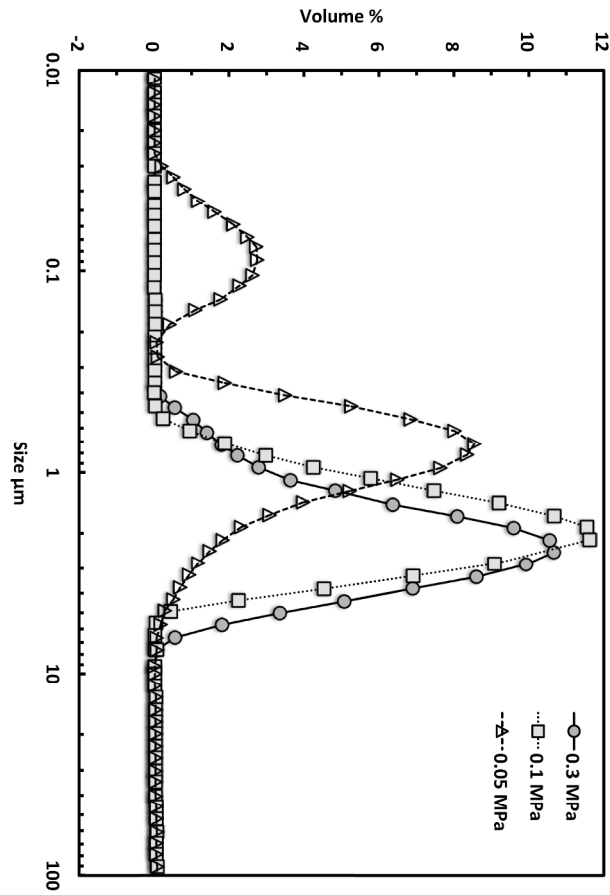


Figure 2. Droplet size distribution data for three emulsion samples (Table 3: A, B & C) produced using a 0.2 μm pore membrane with a fixed velocity for the cross-flowing continuous phase of 2 m/s, and at different cross-membrane pressures, as shown.
297x420mm (300 x 300 DPI)

1
2
3
4
5
6
7
8
9
10
11
12
13
14
15
16
17
18
19
20
21
22
23
24
25
26
27
28
29
30
31
32
33
34
35
36
37
38
39
40
41
42
43
44
45
46
47
48
49
50
51
52
53
54
55
56
57
58
59
60

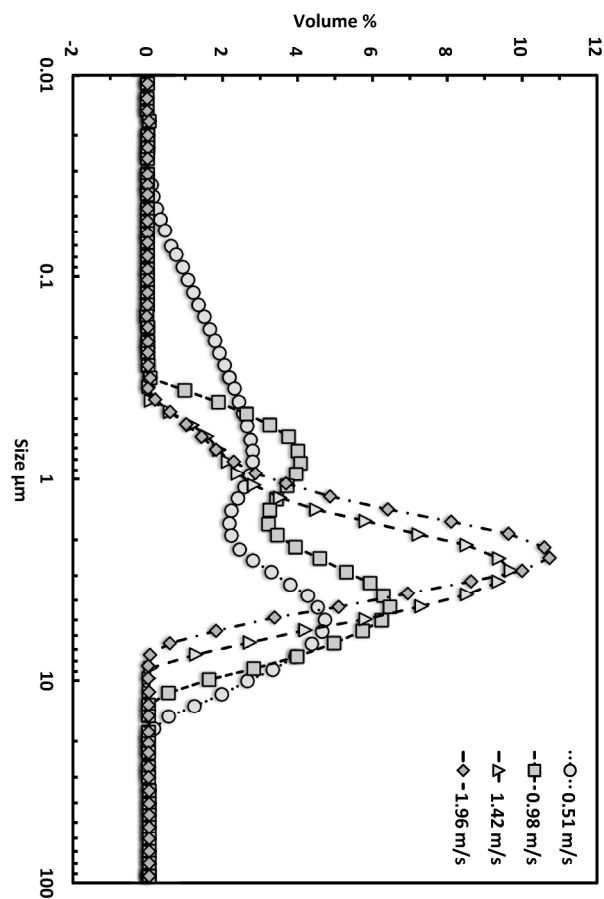


Figure 3. Droplet size distribution data for four emulsion samples (Table 3: C, D, E & F) produced using a 0.2 μm pore membrane with a fixed cross-membrane pressure of 0.3 MPa, and at four cross-flow velocities for the continuous phase, as shown.
297x420mm (300 x 300 DPI)

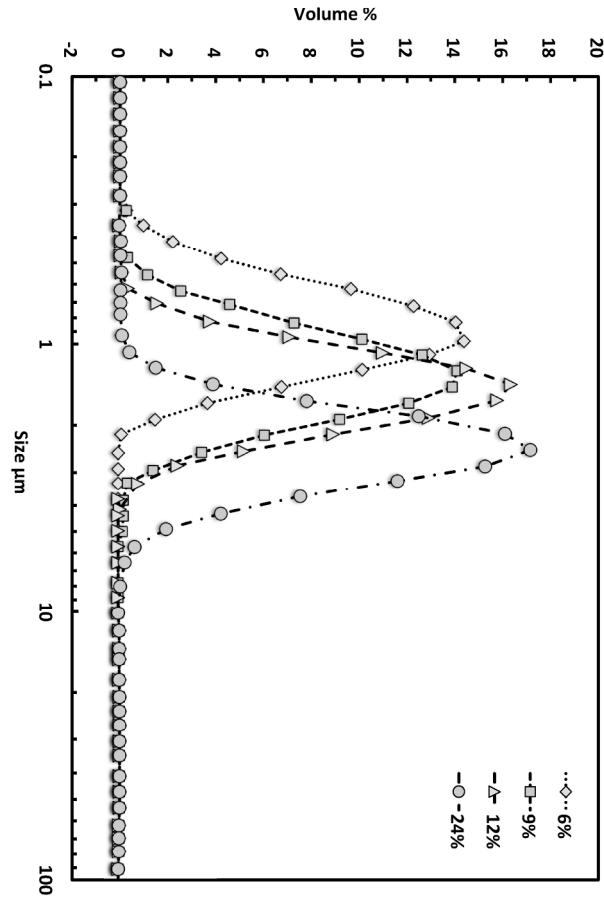


Figure 4. Droplet size distribution data for four emulsion samples (Table 3: G, H, I & J) with differing ratios of MMA to castor oil (as shown) produced at fixed cross-membrane pressure and continuous phase cross-flow conditions.
297x420mm (300 x 300 DPI)

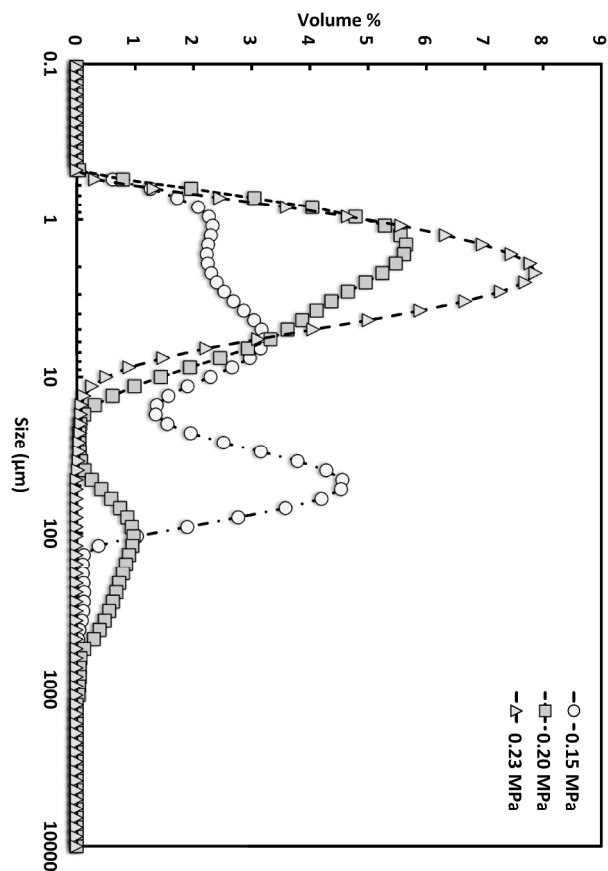


Figure 5. Droplet size distribution data for three emulsion samples (Table 3: K, L & M) produced using a 3 μm pore membrane with a fixed velocity for the cross-flowing continuous phase of 2 m/s, and at different cross-membrane pressures, as shown.
297x420mm (300 x 300 DPI)

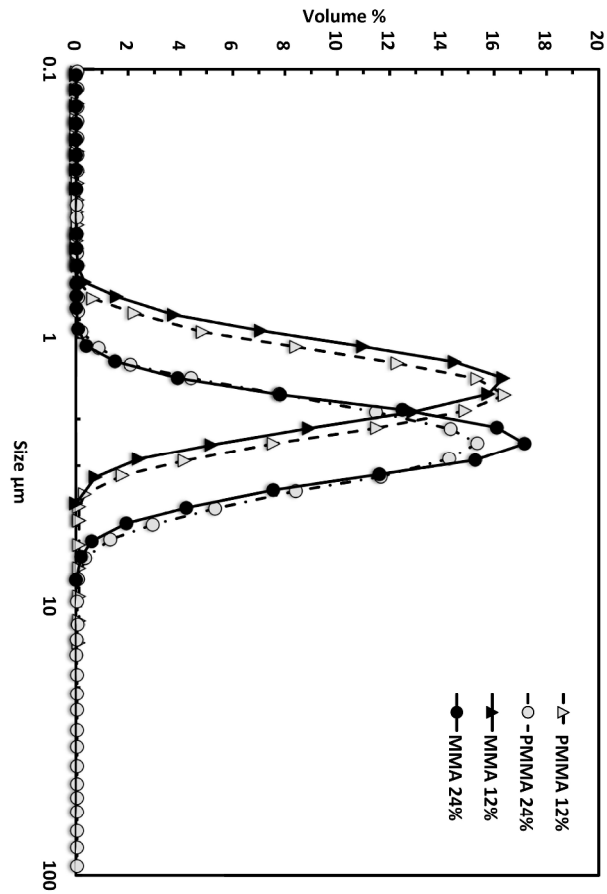


Figure 6. Size distribution data for PMMA/CO microcapsule particle samples and relevant pre-cursor emulsions produced using a 0.2 µm pore membrane (Table 3: I & J).
297x420mm (300 x 300 DPI)

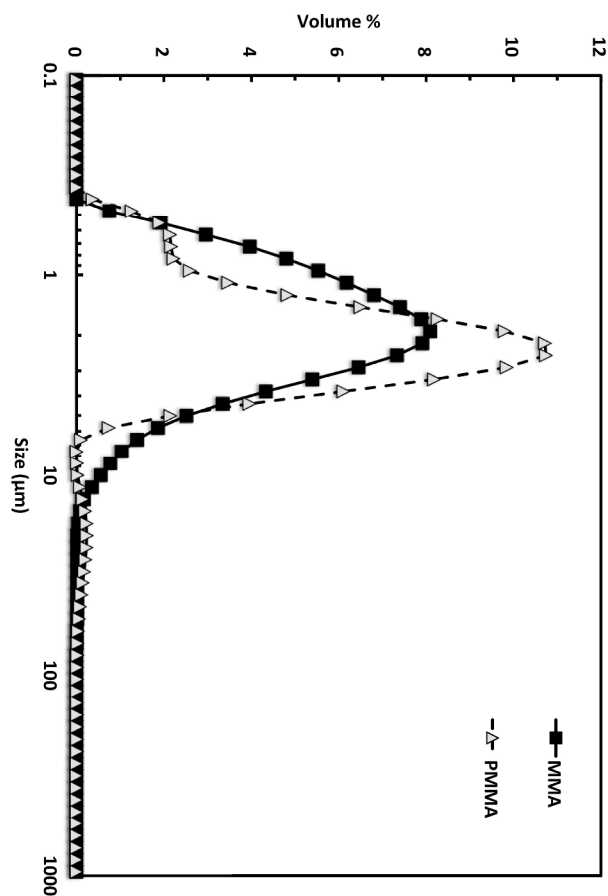
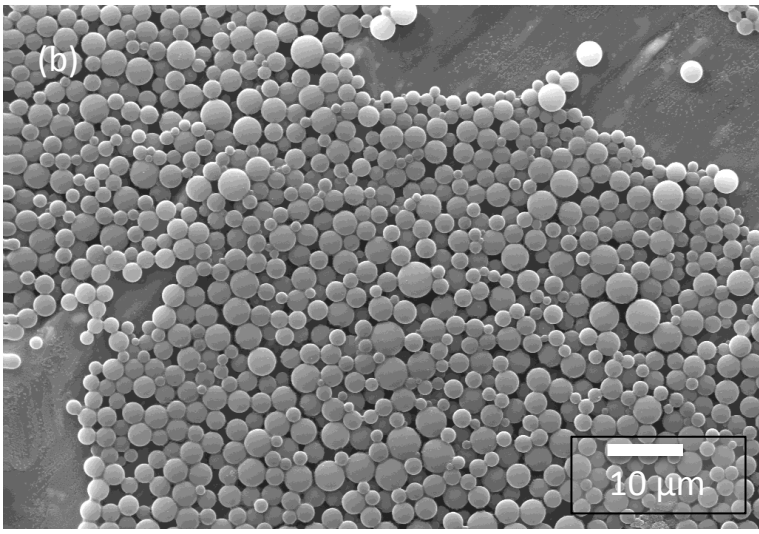
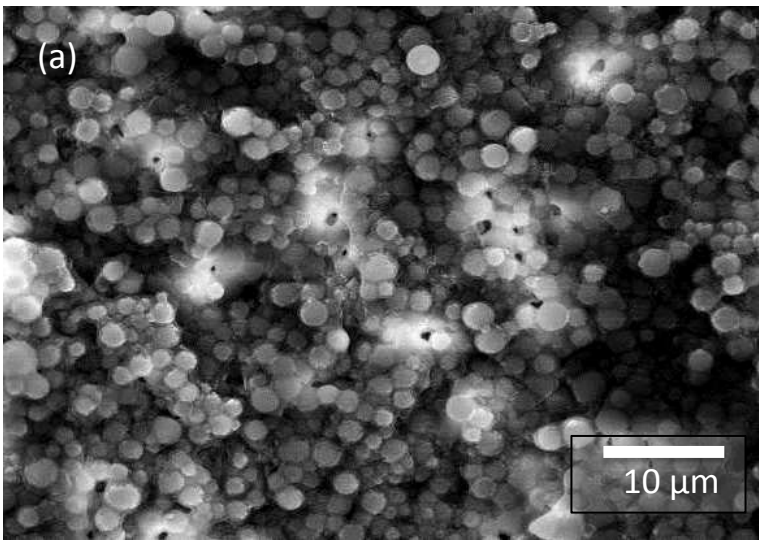


Figure 7. Size distribution data for a solid PMMA particle sample and the corresponding pre-cursor emulsion produced using a 3 µm pore membrane (Table 3: M).
297x420mm (300 x 300 DPI)

1
2
3
4
5
6
7
8
9
10
11
12
13
14
15
16
17
18
19
20
21
22
23
24
25
26
27
28
29
30
31
32
33
34
35
36
37
38
39
40
41
42
43



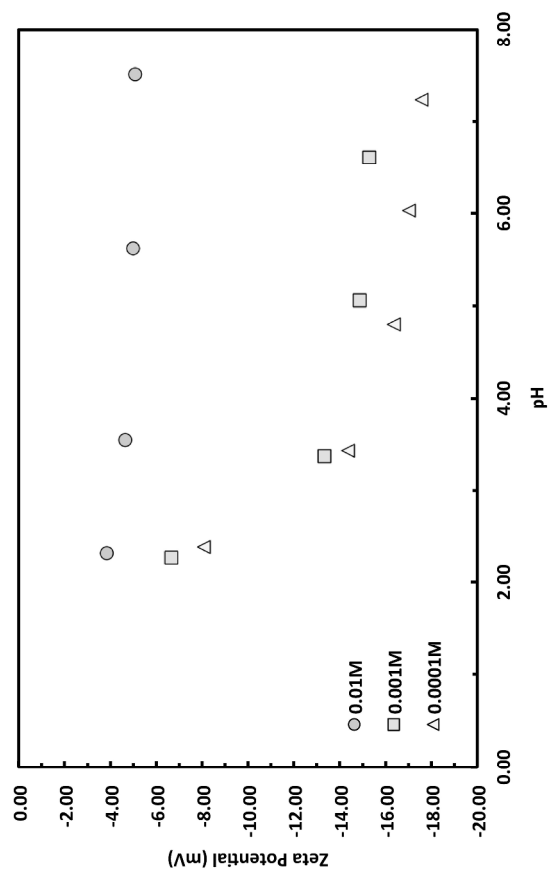


Figure 9. Zeta potential as a function of pH for the solid PMMA particle sample at three different background salt concentrations as marked on the figure.
297x420mm (300 x 300 DPI)

Table 1:

# ¹	Hydroquinone Concentration (wt% to total emulsion)	NaSO ₃ Concentration (wt% to total emulsion)	Polymerisation Duration (hours)	Final Polymer Concentration (wt%) ²	Dispersion Characteristics
1	0	0	3	30	White, thick, magnetic stirrer eventually stopped, solid lumps of coagulum forming around it
2	0	0	20	35	White, very thick, magnetic stirrer eventually stopped, solid lumps of coagulum forming around it
3	0.02	0	8	3	Yellow, very oily, separated
4	0.03	0	24	16	Yellow, oily blobs, separated
5	0.03	0.02	24	27	Beige, very thick, magnetic stirrer eventually stopped, solid lumps of coagulum forming around it
6	0.15	0	24	12	Yellow, oily blobs, separated

1. Each formulation had the same base water/SDS/MMA/LA content at 1553 g/0.7 g/750 g/37.5 g
2. Polymerisation was initiated at 65 °C using 1.5 g BPO

Table 2:

MMA Emulsion [XME] (g)	
Disperse Phase	
MMA	750.0
LA	37.5
BPO	15.0
Continuous Phase	
Water	1552.5
SDS	10.4
PVA	15.0
Total mass	2380.4

For Review Only

Table 3:

Sample Run	Formulation	Experimental conditions				Droplet Properties		Weber Number ² (disperse)	Capillary Number ² (continuous)
		Membrane Pore (μm)	Membrane pressure (MPa)	Disperse phase flux ($\text{L}/\text{m}^2\cdot\text{h}$)	Continuous phase cross-flow (m/s)	D50 (μm) ¹	Span		
A	MMA	0.2	0.05	11	2	0.9, 0.1		1.5×10^6	1.79
B	MMA	0.2	0.1	33	2	2.4	1.2		
C	MMA	0.2	0.3	66	2	3.1	1.4		
D	MMA	0.2	0.3	60	1.5	2.4	1.5		1.34
E	MMA	0.2	0.3	57	1	1.0, 5.1			0.89
F	MMA	0.2	0.3	56	0.5	1.1, 7.0			0.45
G	MMA / CO 6%	0.2	0.3	65	2	0.9	0.6		
H	MMA / CO 9%	0.2	0.3	65	2	1.2	1.7		
I	MMA / CO 12%	0.2	0.3	64	2	1.4	1.3		
J	MMA / CO 24%	0.2	0.3	66	2	2.5	1.5		
K	MMA	3	0.15	273	2	0.9, 5.8, 46			
L	MMA	3	0.20	684	2	1.3, 91			
M	MMA	3	0.23	3,650	2	2.0	2.0	2.3×10^3	1.79
N	MMA	10	0.23	10,945	2	3.1	2.7	6.8×10^2	1.79

1. True values of D50 along with the span are given only for samples with a monomodal size distribution. Approximate values of the mean size for each peak are given for multi-modal samples.
2. Assumes an interfacial tension of 1 mN/m based on SDS data from [29].

1
2
3
4
5
6
7
8
9
10
11
12
13
14
15
16
17
18
19
20
21
22
23
24
25
26
27
28
29
30
31
32
33
34
35
36
37
38
39
40
41
42
43
44
45
46
47
48
49

For Review Only